

Fermi surface evolution and Luttinger theorem in Na_xCoO_2 : a systematic photoemission study

H.-B. Yang,¹ Z.-H. Pan,¹ A.K.P. Sekharan,¹ T. Sato,² S. Souma,² T. Takahashi,²

R. Jin,³ B.C. Sales,³ D. Mandrus,³ A.V. Fedorov,⁴ Z. Wang,¹ and H. Ding¹

(1) Department of Physics, Boston College, Chestnut Hill, MA 02467

(2) Department of Physics, Tohoku University, 980-8578 Sendai, Japan

(3) Condensed Matter Science Division, Oak Ridge National Laboratory, Oak Ridge, TN 37831

(4) Advanced Light Source, Lawrence Berkeley National Laboratory, Berkeley, CA 94720

We report a systematic angle-resolved photoemission study on Na_xCoO_2 for a wide range of Na concentrations ($0.3 \leq x \leq 0.72$). In all the metallic samples at different x , we observed (i) only a single hole-like Fermi surface centered around Γ and (ii) its area changes with x according to the Luttinger theorem. We also observed a surface state that exhibits a larger Fermi surface area. The e'_g band and the associated small Fermi surface pockets near the K points predicted by band calculations are found to “sink” below the Fermi energy in a manner almost independent of the doping and temperature.

The surprising discovery of superconductivity on $\text{Na}_x\text{CoO}_2 \cdot y\text{H}_2\text{O}$ [1] raises many interesting questions on the nature of pairing and its connection to the high- T_c superconductivity. The phase diagram of the cobaltate $\text{Na}_x\text{CoO}_2 \cdot y\text{H}_2\text{O}$, with varying electron doping x and water intercalation y over a wide range, is very rich and complicated. In addition to superconductivity, it exhibits charge order, magnetic order including a metamagnetic transition, and other structural transitions [2, 3, 4, 5]. The physics of these phases and the transitions among them is of importance by itself, and offers an excellent platform for studying correlated triangular lattice fermion systems.

Understanding the evolution of the low-energy electronic structure such as the quasiparticle (QP) dispersion and the Fermi surface (FS) topology is a necessary step toward understanding the diverse physical properties and the nature of the pairing interaction in this class of transition metal oxide. It is therefore important to gain the precise knowledge of the FS structure and the low-energy excitations in the unhydrated Na_xCoO_2 which have been the focus in many recent theoretical and experimental efforts. The cobaltate is a multi-orbital system where the Co^{4+} is in the $3d^5$ configuration, occupying the lower t_{2g} band complex similar to the ruthenate Sr_2RuO_4 . First principle band calculations have predicted that Na_xCoO_2 has a large FS associated with the a_{1g} band centered around the Γ point and six small FS pockets of mostly e'_g character near the K points for a wide range of x [6, 7]. Based on this band structure, it has been proposed that the large density of states contribution from the six FS pockets and the nesting condition among them enhance the spin fluctuations and lead to superconducting pairing of the QPs on these FSs [8]. However, angle-resolved photoelectron spectroscopy (ARPES) measurements on the cobaltate with high Na concentrations ($x \sim 0.6 - 0.7$) revealed only the large FS [9, 10]. It was also noticed that the enclosed FS area, i.e. the density of holes, may not satisfy the Luttinger theorem which is a fundamental QP counting rule in interacting electron systems. It

is therefore desirable to study the evolution of the QP band dispersion and the FS, especially the fate of the FS pockets as a function of the Na concentration x . This is the focus of this work. We choose a set of metallic Na_xCoO_2 with $0.3 \leq x \leq 0.72$. The insulating phase at $x = 0.5$ due to Na dopant order and the magnetic phase at $x \geq 0.75$ are outside the scope of this study.

High quality single crystal Na_xCoO_2 samples were prepared by the flux method and subsequent sodium deintercalation. ARPES experiments were performed at the Synchrotron Radiation Center, WI, and the Advanced Light Source, CA. High-resolution undulator beamlines and Scienta analyzers with a capability of multi-angle detection have been used. Most spectra were measured using 100 eV photons which we found to suit well for the FS mapping of Co $3d$ orbitals. However, some spectral features are better revealed at lower photon energies which will be discussed below. The energy resolution is $\sim 10 - 40$ meV, and the momentum resolution $\sim 0.02 \text{ \AA}^{-1}$. Samples are cleaved and measured *in situ* in a vacuum better than $8 \times 10^{-11} \text{ Torr}$ at low temperatures (20 - 40 K) on a flat (001) surface.

Due to the surface-sensitive nature of ARPES, extra care needs to be taken in assessing how much ARPES data represent the bulk electronic structure. In many cases, surface states arise from surface reconstruction. One useful way to distinguish the surface state from the bulk state is to utilize the property that the surface state is more sensitive to surface disorder. The technique used in the ARPES community is to thermally cycle a sample and thus introduce disorder to the surface. This method is often found to be very effective in removing the surface state in Sr_2RuO_4 [11, 12]. On a freshly cleaved Na_xCoO_2 surface, we often observed an unusual double-band dispersion [10], as shown in Fig. 1(a). However, after the thermal cycle (40 K - 200 K - 40 K), one of the two bands (labeled as “S” in Fig. 1) disappears, which is likely a surface state. We note that this surface state has a larger Fermi vector (k_F) and a smaller Fermi velocity (v_F). The “surviving” band (labeled as “B”) is likely

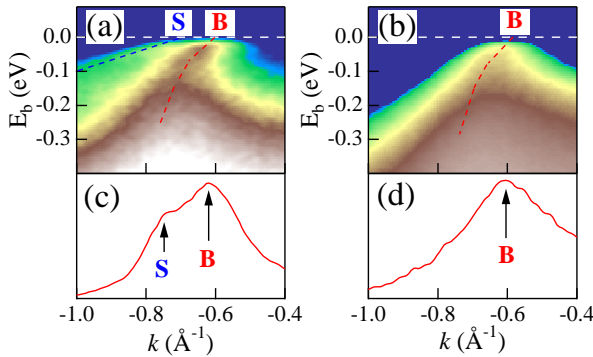


FIG. 1: ARPES E - k intensity plots at $T = 40$ K on (a) a fresh surface of $\text{Na}_{0.72}\text{CoO}_2$ and (b) an aged surface of the same sample after a thermal cycle to 200 K. Red dashed lines are guides for the bulk band (marked as “B”), and the blue dashed line in (a) traces the surface state (marked as “S”). The lower panel shows the momentum distribution curves at E_F obtained on (c) the fresh surface and (d) the aged surface where the surface state vanishes.

bulk-representative. Throughout the paper, we will only discuss the bulk-like band structure. The bulk nature of the ARPES data reported here is further verified by our x-ray ARPES which has much longer escape length for photoelectrons. The reason we use lower photon energy here is that it has much better resolutions in both energy and momentum, which enable us to study the FS and low-energy excitations more precisely.

We start with a survey of the valence bands and its doping dependence, as shown in Fig. 2. Panels (a) and (b) show the second derivative intensity (SDI) plots (a common practice to display dispersion for broad peaks) along Γ - M for $x = 0.48$ and 0.72 , respectively. There are four major band branches, with the one at ~ 0.5 eV being assigned to the Co $3d$ t_{2g} orbitals, and the other three at $\sim 3, 4.5, 6$ eV to the O $2p$ orbitals, according to local density approximation (LDA) calculation [6]. The comparison between the two doping levels, plotted in Fig. 2(c), shows a clear and non-trivial doping dependence on the energy level of these bands. For the Co $3d$ orbitals, the average energy difference between the two doping levels is ~ 0.1 eV, which is likely due to a shift of the chemical potential caused by the change of carrier numbers. However, for the O $2p$ orbitals, the energy shifts (~ 0.5 eV) between the two doping levels are larger. We note that this doping dependence of the O- $2p$ orbitals can explain well the doping-dependent shift of the α peak in optical conductivity measurement which is associated with the transition from the fully occupied O- p states to the unoccupied Co e_g states [13].

Zooming in on the Co- $3d$ orbitals, one can identify more dispersive features. Figs. 2 (d) and (e) display the SDI plots of $\text{Na}_{0.35}\text{CoO}_2$ on a smaller energy scale (~ 1.5 eV) along Γ - M and Γ - K directions, respectively. By comparing to the LDA band structure for the same Na content [7], one can assign orbital characters to the dispersive features. However, the measured occupied band-widths (~ 0.7 - 0.8 eV) are, remarkably, narrower than

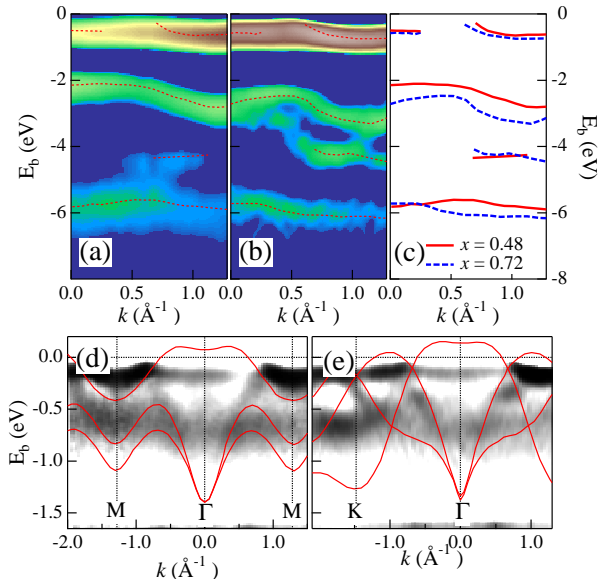


FIG. 2: SDI plots of the valence bands along Γ - M for (a) $x = 0.48$ and (b) $x = 0.72$. Red dashed lines are the guides for band dispersion. (c) Comparison of Co- $3d$ and O- $2p$ orbitals between $x = 0.48$ and $x = 0.72$. The lower panel shows the SDI plots for the Co- $3d$ orbitals in $\text{Na}_{0.35}\text{CoO}_2$ along (d) Γ - M and (e) Γ - K . Red lines are band dispersions from the LDA calculation [7].

the calculated ones (1.3 - 1.4 eV), resulting in approximately a factor of two in the overall bandwidth reduction, indicating the importance of strong electron correlations in this material. Note that the flat features at the unoccupied wavevectors (k) visible in Figs. 2(d) and (e) near the Fermi energy (E_F) may be due to the incoherent background often observed in correlated materials.

To study the low-energy excitations and the FS more closely, we further zoom in near E_F (within 0.2 eV), as shown in Fig. 3 where a sample of $\text{Na}_{0.48}\text{CoO}_2$ is measured. This time we directly display the intensity plots since the near- E_F features are much sharper (see the energy distribution curves (EDCs) in Fig. 3(a)), and the SDI plot cannot reveal the near- E_F band well due to the interference of the Fermi-Dirac function. During the ARPES measurement, we took many parallel cuts (five of them are shown in Figs. 3 (b) - (f)) in k space. It is important to have such long cuts that cover several Brillouin zones (BZs) in order to accurately determine the FS, since they can help eliminate many potential problems such as sample misalignment and matrix element effects. Indeed, we have a small misalignment of about 3° in this sample as can be seen in Fig. 3(g). Note that the intensity is much weaker in the 2nd BZ due to the photoemission matrix element effect. The FS is determined by plotting the ARPES intensity within a narrow energy window (± 2 meV) at E_F in the two-dimensional (2D) k space as shown in Fig. 3(g) where partial FS contours over two BZs are extracted from the five long cuts shown above. We also note that the low-energy band is further renormalized due to a strong “kink” in the dispersion observed at the energy scale of 70 - 100 meV

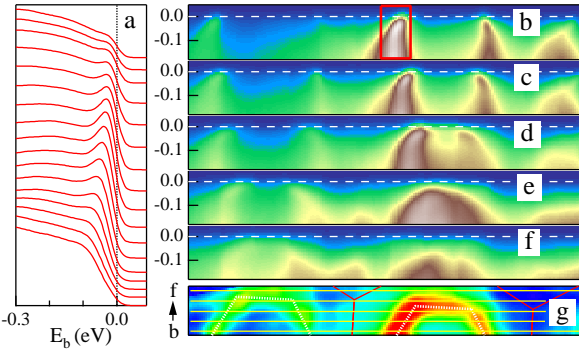


FIG. 3: An example of the FS mapping on $\text{Na}_{0.48}\text{CoO}_2$. (a) Representative EDCs within the red box in panel (b). (b) - (f) E - k intensity plots along the long cuts indicated by the yellow solid lines in panel (g) where FS contours obtained from the intensity at E_F , and BZ boundaries (thin red hexagons), are plotted. White dashed lines are the guides for the FSs.

(see Figs. 3(b) - (d)). The behavior of this “kink” and the relationship to the well-known “kink” in the dispersion observed in high- T_c cuprates [14, 15, 16, 17] will be discussed in a separate publication.

The FS we observed, as shown in Fig. 3(g), corresponds to the large a_{1g} FS centered at the Γ point predicted by the LDA calculation [6]. However, the six small FS pockets associated with the e'_g band predicted by the LDA are not present in our measurements for the entire range of $0.3 \leq x \leq 0.72$. Instead, we observed a broad peak that approaches but never reaches E_F near the K points, as indicated by the black triangles in Fig. 4(a). In addition, we observed two more dispersive features. The one indicated by the green triangles belongs to the a_{1g} band, and the other indicated by the blue triangles is assigned to the other e'_g band. The reason that the intensity of the a_{1g} band is much weaker in Fig. 4 than in Fig. 3 is that different photon energies were used in the two measurements. While we used 100-eV photons in Fig. 3 to enhance the Co-3d character, we found that the e'_g band near the K points is greatly enhanced at lower photon energies (30 eV in Fig. 4). This may suggest a stronger mixing of O-2p character in the e'_g bands since the O p orbitals are more sensitive to the low-energy photons, a property often observed in the ARPES studies of cuprates.

The broad e'_g bands can be observed more clearly in the SDI plot, as shown in Fig. 4(b). In comparison, the measured dispersions are reminiscent of the e'_g bands calculated by the LDA [6, 7], as shown in Fig. 4(c). However, important differences exist: 1) the measured bandwidth is narrower than the calculated one; 2) the upper branch of e'_g bands does not cross the Fermi level - the predicted FS pockets “sink” below E_F . More significantly, this “sinking” pocket does *not* have doping dependence for its band top, as shown in Fig. 4(c), while the band bottom shifts with doping (~ 100 meV shift between $x = 0.3$ and $x = 0.48$). This behavior reminds us of the leading edge property associated with the opening of an energy gap at the FS. However, we did not observe clear leading-edge shift for temperatures up to 250 K.

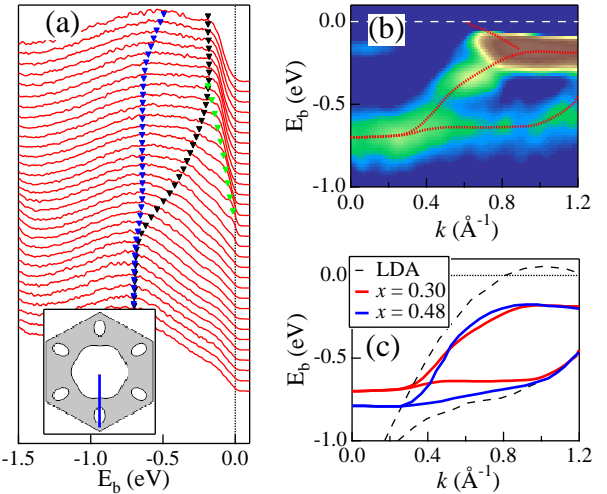


FIG. 4: “Sinking” pockets near the K points. (a) EDCs of $\text{Na}_{0.3}\text{CoO}_2$ along Γ - K measured using 30 eV photons. Triangular markers are the guides for the band dispersion. The insert shows the location of the cut in the BZ. (b) SDI plot for the same measurement. Red dashed lines, representing the triangular markers in panel (a), are the guides for the dispersion. (c) A comparison of the measured e'_g bands at $x = 0.3$ (red solid lines) and 0.48 (blue solid lines) to the LDA calculation [7] (black dashed lines).

We summarize our ARPES results on the FS evolution in Na_xCoO_2 in Fig. 5. We have measured many samples and obtained well-reproducible results over a wide range of Na concentrations. Figs. 5(a) - (c) show three examples of the measured FS for $x = 0.3, 0.48$, and 0.72. Clearly, a single hexagonal hole-like FS, centered at the Γ point, shrinks its size as x increases. A direct comparison of the FS contours at the four doping levels, shown in Fig. 5(d), provides more quantitative information on the FS evolution. All Fermi surfaces have a good hexagonal shape with parallel FS edges that can be connected by a nesting vector (\vec{Q}_n). The magnitude of \vec{Q}_n is estimated to be $\sim 1.41, 1.40, 1.20, 1.18 \text{ \AA}^{-1}$ ($\pm 0.1 \text{ \AA}^{-1}$) for $x = 0.3, 0.48, 0.6, 0.72$. Interestingly, these values are close to the reciprocal lattice vectors ΓK (1.47 \AA^{-1}) and ΓM (1.28 \AA^{-1}). From Fig. 5(d), we derive the carrier density from the FS area which we call the “effective Na concentration” $x' = 1 - 2A_{FS}/A_{BZ}$, where A_{FS} is the area enclosed by the 2D FS, and A_{BZ} is the area of the BZ. In Fig. 5(e), x' is plotted vs the nominal Na concentration x . If the Luttinger theorem is satisfied, one has $x' = x$, which is indicated by the solid line in Fig. 5(e). Within the experimental uncertainties, Fig. 5(e) shows that x' tracks well the $x' = x$ line and the Luttinger theorem is thus satisfied. The conservation of the doped electron density is quite remarkable and is consistent with the non-existence of the small FS pockets. In contrast, the FS pockets near the K points predicted by LDA calculations contribute to a significant portion of the total FS area at low doping. This helps clarify the puzzle of the FS being too large in previous ARPES results [9, 10]. A part of the reason for this discrepancy, besides the issue

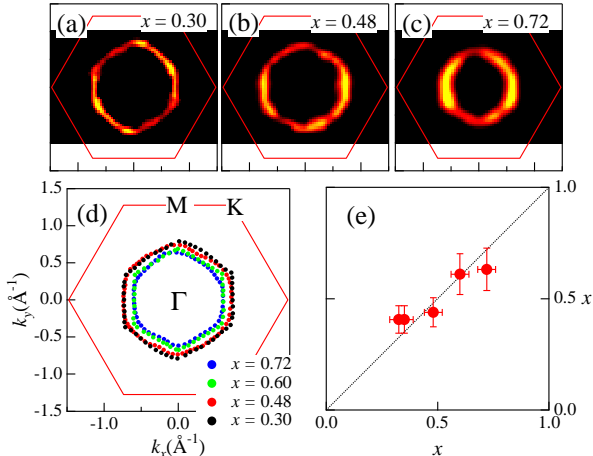


FIG. 5: FS evolution in Na_xCoO_2 . (a) - (c) FSs (the intensity contours at E_F) for $x = 0.3$, 0.48 , and 0.72 in the first BZ (red solid lines). (d) Overlap of the FS locations at four doping levels in the BZ. (e) Effective Na concentration x' derived from FS area *v.s.* Na concentration x . The diagonal line is from the Luttinger theorem.

of experimental accuracy, is that we eliminated the surface state in this study, which is tied to a larger FS as discussed above. We note that there may exist a small jump in the FS area across $x = 0.5$, as shown in Figs. 5(d) and (e). It is known that the metallic states of Na_xCoO_2 are different across $x = 0.5$, with Pauli-like susceptibility for $x < 0.5$ and Curie-Weiss like for $x > 0.5$. Whether the jump is real or how it relates to the magnetic “transition” is still an open question that needs further investigation.

The observation of the “sinking” pockets near the K points for such a wide range of Na concentrations is very intriguing. The qualitative discrepancy with the LDA band structure points to the importance of electronic correlation effects and is a basic unresolved issue in understanding the physical properties of the cobaltates. A recent theoretical work based on the local spin density approximation (LSDA) takes into account the local Coulomb repulsion (U) using the LSDA+ U approach and finds the absence of the small FS pockets [18]. How-

ever, the disappearance of the small FS pockets in the LSDA calculation is due to the formation of a half-metal with spin-split bands and spin polarized FSs, resulting in a FS area twice as large which is inconsistent with our observations. The observed behavior that the top of the “sinking” pocket stays at the same energy while sizable energy shifts appear at the band bottom for different doping levels is unusual and seems to suggest either the opening of a gap or more intricate many-body effects. So far, the lack of the temperature dependence of the leading edge does not appear to support the gap-opening scenario. A better understanding of the correlation effects as well as those associated with the crystal field splitting and the hybridization with the O- $2p$ orbitals is clearly needed in order to understand these unconventional electronic properties.

In conclusion, our ARPES results on Na_xCoO_2 over a wide range of Na concentrations ($0.3 \leq x \leq 0.72$) clearly show that there is only a single hexagonal FS centered around the Γ point, with parallel edges being possibly nested. We find that the evolution of this hole-like FS obeys the Luttinger theorem. The small FS pockets near the K points predicted by the LDA calculations are found to “sink” below E_F with a distance to the Fermi sea almost independent of doping and temperature. These findings provide clear and detailed knowledge of the evolution of the electronic structure in Na_xCoO_2 and put constraints on the theoretical description of the superconductivity in the hydrated cobaltates.

We thank P.A. Lee, D.J. Singh for valuable discussions and suggestions, and S. Gorovikov, H. Höchst for technical support in synchrotron experiments. This work is supported by NSF DMR-0353108, DOE DE-FG02-99ER45747, Petroleum Research Fund, and the MEXT of Japan. This work is based upon research conducted at the Synchrotron Radiation Center supported by NSF DMR-0084402, and at the Advanced Light Source supported by DOE DE-AC03-76SF00098. Oak Ridge National laboratory is managed by UT-Battelle, LLC, for DOE under contract DE-AC05-00OR22725.

[1] K. Takada *et al.*, *Nature* **422**, 53 (2003).
[2] M.L. Foo *et al.*, *Phys. Rev. Lett.* **92**, 247001 (2004).
[3] J.L. Luo *et al.*, *Phys. Rev. Lett.* **93**, 187203 (2004).
[4] B.C. Sales *et al.*, *Phys. Rev. B* **70**, 174419 (2004).
[5] Q. Huang *et al.*, *Phys. Rev. B* **70**, 134115 (2004).
[6] D.J. Singh, *Phys. Rev. B* **61**, 13397 (2000).
[7] K.-W. Lee *et al.*, *Phys. Rev. B* **70**, 045104 (2004).
[8] M.D. Johannes *et al.*, *Phys. Rev. Lett.* **93**, 097005 (2004).
[9] M.Z. Hasan *et al.*, *Phys. Rev. Lett.* **92**, 246402 (2004).
[10] H.-B. Yang *et al.*, *Phys. Rev. Lett.* **92**, 246403 (2004).
[11] A. Damascelli *et al.*, *Phys. Rev. Lett.* **85**, 5194 (2000).
[12] S.-C. Wang *et al.*, *Phys. Rev. Lett.* **92**, 137002 (2003).
[13] N.L. Wang *et al.*, *Phys. Rev. Lett.* **93**, 237007 (2004).
[14] T. Valla *et al.*, *Science* **285**, 2110 (1999).
[15] P.V. Bogdanov *et al.*, *Phys. Rev. Lett.* **85**, 2581 (2000).
[16] A. Kaminski *et al.*, *Phys. Rev. Lett.* **86**, 1070 (2001).
[17] A. Lanzara *et al.*, *Nature* **412**, 510 (2001).
[18] Peihong Zhang *et al.*, *Phys. Rev. Lett.* **93**, 236402 (2004).